JACS
JOURNAL OF THE AMERICAN CHEMICAL SOCIETY
Article
pubs.acs.org/JACS

# Dynamic Nuclear Polarization of $^{1}H$, $^{13}C$, and $^{59}Co$ in a Tris(ethylenediamine)cobalt(III) Crystalline Lattice Doped with Cr(III)

Björn Corzilius,[†,§,⊥] Vladimir K. Michaelis,[†,⊥] Susanne A. Penzel,[†,∥] Enrico Ravera,[†,‡] Albert A. Smith,[†,∥] Claudio Luchinat,*[,‡] and Robert G. Griffin*[,†]

[†]Francis Bitter Magnet Laboratory and Department of Chemistry, Massachusetts Institute of Technology, 77 Massachusetts Avenue, Cambridge, Massachusetts 02139, United States

[‡]Center for Magnetic Resonance and Department of Chemistry "Ugo Schiff", University of Florence, 6 Via Luigi Sacconi, 50019 Sesto Fiorentino, Italy

Supporting Information

**ABSTRACT:** The study of inorganic crystalline materials by solid-state NMR spectroscopy is often complicated by the low sensitivity of heavy nuclei. However, these materials often contain or can be prepared with paramagnetic dopants without significantly affecting the structure of the crystalline host. Dynamic nuclear polarization (DNP) is generally capable of enhancing NMR signals by transferring the magnetization of unpaired electrons to the nuclei. Therefore, the NMR sensitivity in these paramagnetically doped crystals might be increased by DNP. In this paper we demonstrate the possibility of efficient DNP transfer in polycrystalline samples of $[Co(en)_3Cl_3]_2{\cdot}NaCl{\cdot}6H_2O$ (en = ethylenediamine, $C_2H_8N_2$) doped with Cr(III) in varying concentrations between 0.1 and 3 mol %. We demonstrate that $^{1}H$, $^{13}C$, and $^{59}Co$ can be polarized by irradiation of Cr(III) with 140 GHz microwaves at a magnetic field of 5 T. We further explain our findings on the basis of electron paramagnetic resonance spectroscopy of the Cr(III) site and analysis of its temperature-dependent zero-field splitting, as well as the dependence of the DNP enhancement factor on the external magnetic field and microwave power. This first demonstration of DNP transfer from one paramagnetic metal ion to its diamagnetic host metal ion will pave the way for future applications of DNP in paramagnetically doped materials or metalloproteins.

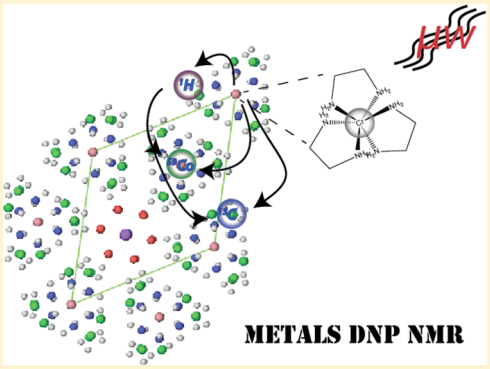


## INTRODUCTION

The number and variety of applications of high-field dynamic nuclear polarization (DNP) have increased significantly during the past few years,[1] primarily because microwave-driven DNP is widely applicable and capable of enhancing NMR signals by several orders of magnitude. Microwave-driven DNP therefore dramatically reduces the acquisition times of many lengthy experiments.[2,3] Accordingly, high-field magic-angle spinning (MAS) DNP has been used by many groups to examine samples where the analyte and a stable paramagnetic polarizing agent, usually a $g \approx 2$ organic radical, are dissolved in a glass-forming mixture (typically 60/40 v/v glycerol/water).[4−12] The spin system is then irradiated with high-frequency microwaves, which enables the transfer of electron polarization to nuclear spins, leading to an enhanced NMR signal. With this approach, the best overall results have been achieved when the analyte is homogeneously dispersed within the glass (e.g., membrane proteins, amyloid fibrils, or microcrystals).[13−25]

The appearance of commercially available high-field DNP instrumentation has also stimulated the development of additional approaches to produce suitable paramagnetic samples.[13,17,21,24,26−28] Many of these studies have focused on the cross effect (CE) as well as approaches required to optimize the enhancements. In addition, mechanistic studies have renewed interest in the solid effect (SE)[29−31] and demonstrated that high-power microwave (mw) sources can increase the enhancement of the SE to the point where it is competitive with the CE.[32] In parallel, new and improved polarizing agents for both the SE and CE have appeared.[33−42]

The introduction of paramagnetic transition-metal and rare-earth ions as polarizing agents for the SE[42] and for the Overhauser effect (OE) in solution[43] demonstrated the possibility of applying DNP to a variety of samples that contain intrinsic paramagnetic metal sites or can be easily doped with those species. This approach is applicable to a large collection of paramagnetic metalloproteins and enzymes, and also to a group of crystalline (inorganic) materials containing paramagnetic dopants or defects. These materials often occur naturally (e.g., ruby, $Al_2O_3{:}Cr^{3+}$), or can be synthesized by substituting a diamagnetic host ion with a paramagnetic analogue (i.e., a d- or f-block metal center);[44] additionally, unpaired electrons can be found in F centers (i.e., Farbzentren or color centers, anionic vacancies in the lattice that are occupied by electrons)[45−47] or other defects where dopants substitute a host site with a mismatch in the number of valence

**Received:** May 6, 2014
**Published:** July 29, 2014

electrons, such as diamond NV centers, which feature interesting spin properties.[48−50] Doping with paramagnetic species often does not significantly alter the physical properties of the host material if the host ion and the dopant have similar properties (i.e., charge and ionic size), and therefore, it is an ideal tool to study the properties of the pristine (diamagnetic) materials using paramagnetic techniques.

Paramagnetically doped inorganic systems have been investigated extensively with electron paramagnetic resonance (EPR) spectroscopy, but their characterization by NMR spectroscopy remains a challenge,[51−57] as the target diamagnetic metals may have nonfavorable nuclear properties, including a quadrupolar interaction ($I > {}^1/_2$, i.e., quadrupolar broadening), or suffer from low natural abundance and/or low gyromagnetic ratio. These properties reduce the overall sensitivity and when combined often require complicated experimental methods and extended acquisition times.[58,59] The presence of paramagnetic doping in these systems makes them appealing for applications of DNP, which offers the ability to boost the nuclear polarization and reduce the experiment time. However, in these cases both the polarization source (paramagnetic dopant) and the target (diamagnetic host ion) are often considered nonideal systems for DNP spectroscopy. Typically, organic $S = {}^1/_2$ radicals for the SE (e.g., trityl,[60] BDPA[34,61]) or specifically tailored biradicals for the CE (e.g., TOTAPOL,[62] AMUPol[63]) as well as $I = {}^1/_2$ nuclei (e.g., $^1$H, $^{13}$C, $^{15}$N, $^{29}$Si) are seen as being "ideal" for mechanistic studies and have been used successfully in DNP experiments. However, systems having electron and nuclear spins greater than ${}^1/_2$ are much more abundant than systems with $S = {}^1/_2$ and $I = {}^1/_2$ and therefore are of particular interest, especially in materials science and inorganic chemistry. Additionally, quadrupolar nuclei are sensitive probes of their environment as a result of the coupling between the inherent quadrupole moment and the electric field gradient generated by its surroundings—the magnitude of the coupling will be observed within the spectrum accompanied by a specific shape characteristic of local symmetry. In the case of heavy transition metals, further spectral effects from a considerable chemical shift anisotropy (CSA) can be observed, which are extremely sensitive to the local electronic environment.[64] These couplings often lead to broad NMR powder patterns, with increasing complexity when both anisotropic interactions are present.[65−70] However, this information on couplings and shifts is often difficult to obtain because of typically low gyromagnetic ratios and subsequently low spectral sensitivities.[71−75] In order for DNP-enhanced NMR spectroscopy to become a more generally applicable method, it is important to examine these "nonideal" but more practical cases, even if the enhancements are lower than those achieved in "ideal" systems. Therefore, investigating the feasibility of DNP experiments involving direct polarization transfer from an $S > {}^1/_2$ metal site to another diamagnetic nucleus at an $S = 0$, $I > {}^1/_2$ metal site in a doped polycrystalline system is of considerable interest.

Despite the fact that many metals have paramagnetic oxidation states, they often have prohibitively broad EPR lines due to the large spin−orbit coupling and fast electronic relaxation from low-lying excited states, making them unsuitable for DNP.[76] $Gd^{3+}$ and $Mn^{2+}$, which have $S$-term ($L = 0$) ground states and zero first-order spin−orbit coupling, stand out as valid polarizing agents for high-field DNP NMR spectroscopy.[42] A similar situation is encountered for Cr(III) in an octahedral ligand field, where the three d-shell electrons form a $^4A_2$ ground state with vanishing orbital momentum and spin−orbit coupling. This makes Cr(III) complexes with near-octahedral symmetry ideal targets for investigation as DNP polarizing agents in this study.

Besides these cases with vanishing spin−orbit coupling, Cr(V) complexes, obtained in situ from Cr(VI) salts in the presence of diols, have been successfully polarized when used at low magnetic fields and low temperature (i.e., liquid helium temperature).[77−83] Hence, it can be foreseen that their analogous $VO^{2+}$ and Mo(V) complexes could accomplish this task despite their nonzero spin−orbit coupling because these metal ions have a $d^1$ configuration, resulting in a nondegenerate ground state (in the presence of Jahn−Teller distortion and/or low-symmetry components).

In the present paper, we demonstrate that it is possible to utilize DNP to polarize a host crystalline lattice via paramagnetic transition-metal dopants. We are able to observe $^1$H (indirect) and $^{13}$C (direct) DNP-enhanced NMR spectra from the bidentate ethylenediamine ligands, including the ability to directly polarize the $^{59}$Co nucleus of the diamagnetic transition-metal host within the crystalline lattice. This method paves the way for numerous applications of DNP to paramagnetically doped crystalline materials and potentially to (partially) paramagnetic biosolids.

Figure 1 illustrates the (a, b) molecular and (c) long-range packing of the diamagnetic host complex, $[Co(en)_3Cl_3]_2{\cdot}NaCl{\cdot}6H_2O$ (en = ethylenediamine, $C_2H_8N_2$). The Co atom is six-coordinate, surrounded by three bidentate ethylenediamine ligands coordinated through the electron lone pair on the nitrogen atoms. The symmetry of the free $Co(en_3)^{3+}$ molecular cation would appear to be $D_{3d}$, but it decreases to $C_3$ point symmetry within the trigonal $P3$ space group.[84] Cr(III)-doped $[Co(en)_3Cl_3]_2{\cdot}NaCl{\cdot}6H_2O$ is an ideal system for DNP studies in crystalline environments for several reasons: Co(III) can be substituted by the equally charged Cr(III) without significant distortion of the lattice parameters or symmetry because of the rather similar crystal ionic radii (i.e., 0.545 Å for low-spin $Co^{3+}$ vs 0.615 Å for $Cr^{3+}$).[85] While Co(III) is in a low-spin ($S = 0$) $3d^6$ electronic state in the strong octahedral crystal field, Cr(III) exists in a $3d^3$ configuration and is therefore strictly

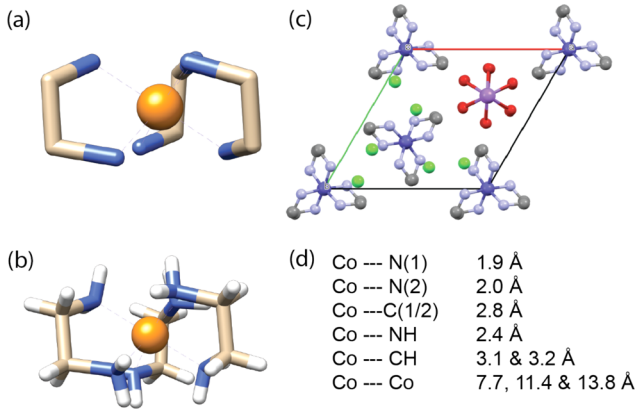


**Figure 1.** Molecular and long-range crystal packing of $[Co(en)_3Cl_3]_2{\cdot}NaCl{\cdot}6H_2O$ (en = ethylenediamine, $C_2H_8N_2$). (a) Molecular unit without hydrogen atoms. (b) Molecular unit with hydrogen atoms. (c) 2D rendering of the crystal structure with the $c$ axis perpendicular to the page. Color scheme: Co, blue; N, light blue; C, gray; Cl, green; Na, purple; O, red. Hydrogen atoms have been removed for clarity. (d) Select interatomic distances determined by X-ray diffraction.[84]


dx.doi.org/10.1021/ja5044374 | J. Am. Chem. Soc. 2014, 136, 11716−11727

paramagnetic ($S = {}^3/_2$). Despite the high-spin state and subsequent occurrence of electron quadrupole coupling [i.e., zero-field splitting (ZFS)], the half-integer spin quantum number results in a narrow EPR $m_S = -{}^1/_2 \leftrightarrow +{}^1/_2$ central transition (CT) suitable for DNP. Furthermore, the variable doping ratio permits tuning of the electron−electron interactions. While the natural isotopic mixture of chromium comprises four different isotopes (4.3% $^{50}$Cr, 83.8% $^{52}$Cr, 9.5% $^{53}$Cr, and 2.4% $^{54}$Cr), only the minority isotope $^{53}$Cr is magnetically active, with a nuclear spin of $I = {}^3/_2$; additionally, the corresponding hyperfine coupling is rather small (about 45 MHz) and does not significantly contribute to the observed line width of the CT. Among Cr complexes, $Cr(en_3)^{3+}$ embedded in $[Co(en)_3Cl_3]_2{\cdot}NaCl{\cdot}6H_2O$ is found to have a small and axially symmetric ZFS.[44,84,86] Cobalt is an isotopically pure element. The $^{59}$Co nucleus has a gyromagnetic ratio close to that of $^{13}$C and can therefore be detected with conventional NMR probes with minor adjustments to the $^{13}$C channel. It has a nuclear spin of $I = {}^7/_2$, and a large quadrupole moment of $Q = 0.42$ barns,[87] although the nuclear quadrupole coupling is small for this complex with $C_3$ symmetry; the CT ($^1/_2 \leftrightarrow -{}^1/_2$) does not suffer from a second-order quadrupolar broadening at rather low magnetic fields of ≥5 T.[88] However, $^{59}$Co does have an extremely sensitive nuclear magnetic shielding that is very sensitive to the polarizability and local chemical bonding environment. Hence, CSA can be a sensitive tool to probe changes in both temperature and chemical structure, as it leads to a large chemical shift range (e.g., a $^{59}$Co chemical shift range of >15 000 ppm; at a field of 5 T, this spans >0.8 MHz).[65,88−91] Besides the metal nuclei (i.e., $Na^+$, $Cr^{3+}$, and $Co^{3+}$), the sample contains the usual complement of $^1$H, $^{13}$C, $^{14}$N, $^{15}$N, and $^{17}$O spins in the organic ligands as well as the counterions ($Cl^-$).

## EXPERIMENTAL SECTION

**Synthesis.** $[M(en)_3Cl_3]_2{\cdot}NaCl{\cdot}6H_2O$ (M = Co, Cr) were prepared according to the protocol of McGarvey[86] by dissolving $Co(en)_3Cl_3{\cdot}2H_2O$ (Sigma-Aldrich) or $Cr(en)_3Cl_3{\cdot}3.5H_2O$ (Strem Chemicals) together with 2.5 g of NaCl per 1 g of complex salt in deionized $H_2O$. The quantity of $H_2O$ was chosen so that the NaCl concentration was slightly below saturation. For the preparation of Cr(III)-doped $[Co(en)_3Cl_3]_2{\cdot}NaCl{\cdot}6H_2O$ with molar doping ratios of 0.1, 0.3, 1, and 3%, portions of the $Cr(en)_3Cl_3$ and $Co(en)_3Cl_3$ solutions were mixed in the appropriate molar ratios. Crystals were obtained by slow evaporation from each of the six solutions (i.e., with 0.1, 0.3, 1, and 3% Cr(III) as well as the 0% and 100% controls). After ∼50% of the solution had evaporated, the crystals were collected using a Büchner funnel with a suction pump and washed with the supernatant. The red-to-orange elongated, needle-shaped crystals with sizes up to several millimeters were then air-dried and ground to a fine powder using an agate mortar and pestle. Crystal structure details for $[Co(en)_3Cl_3]_2{\cdot}NaCl{\cdot}6H_2O$ are summarized in Table S1 in the Supporting Information.

**EPR Spectroscopy.** X-Band (9 GHz) EPR experiments were performed using a Bruker ElexSys E580 spectrometer with a Bruker ER 4118X-MD5 dielectric ring resonator employing a cylindrical $TE_{011}$ mode. Sample temperature control was achieved using a Bruker ER 4118CF-O flow cryostat with liquid helium or liquid nitrogen as the cryogen and an Oxford Instruments ITC 503S temperature controller. A custom-built spectrometer was used for 140 GHz EPR experiments.[92]

**NMR Spectroscopy.** $^{13}$C{$^1$H} cross-polarization (CP) experiments for line width analysis were performed using an 11.7 T (500 MHz, $^1$H) home-built spectrometer (courtesy of D. Ruben, MIT-FBML) with a Chemagnetics (Fort Collins, CO) triple-resonance ($^1$H/$^{13}$C/$^{15}$N) MAS probe equipped with a 4.0 mm Kel-F stator housing. The spinning frequency was set to 10 kHz and regulated with a Bruker (Billerica, MA) MAS controller, and the temperature was maintained at 298 K. The spin lock on $^{13}$C during CP was optimized to match the Hartmann−Hahn condition[96] under MAS with $\gamma B_1/2\pi = 50$ kHz on protons during a contact time of 1.2 ms, which was maintained constant for all samples. Proton pulses and two-pulse phase modulation (TPPM) decoupling[97] were optimized for $\gamma B_1/2\pi = 83$ kHz. All of the spectra were recorded using 512 averaged transients and a recycle delay of 10 s and were referenced externally to adamantane (40.49 ppm with respect to 4,4-dimethyl-4-silapentane-1-sulfonic acid).

**DNP Experiments.** The 211 MHz/140 GHz DNP NMR experiments were performed using a custom-built NMR spectrometer (courtesy of D. Ruben, MIT-FBML) in combination with a custom-built MAS DNP NMR probe featuring a triple-channel radiofrequency circuit and a 140 GHz microwave guide. The probe employs a cryogenic sample exchange and corrugated overmoded waveguide technology to minimize microwave mode conversion and Ohmic losses.[93] The 140 GHz microwaves were generated by a gyrotron oscillator, which provided ∼3−10 W of power at the probe entrance.[94] Sample cooling to 80 K was provided by the cold MAS $N_2$ gas using a custom-built liquid $N_2$ heat exchanger. The temperature was monitored on the outside stator surface by fiber-optic thermometers (Neoptix, Québec, Canada). The field position was swept with a ±750 G superconducting sweep coil and determined with a $^1$H field sweep/lock system.[95]

Powdered samples were packed into 4 mm o.d. sapphire rotors for all of the DNP experiments. The magnetic field was first set to the expected theoretical SE DNP matching condition for each nucleus. DNP enhancements were obtained as the ratio of the NMR signal intensities with microwaves (mw on) and without microwaves (mw off) measured under identical experimental conditions. The magnetic field position was then optimized in order to maximize the enhancement factor.

DNP-enhanced and nonenhanced NMR signal amplitudes were recorded using a $^{13}$C{$^1$H} CP experiment in the case of $^1$H DNP, a direct polarization Bloch decay for $^{13}$C, and a rotor-synchronized Hahn echo (or solid echo) for $^{59}$Co DNP. The spin lock on $^{13}$C during CP was optimized to match the Hartmann−Hahn condition [96] under MAS with $\gamma B_1/2\pi = 100$ kHz on protons during a contact time of 1.5 ms. TPPM $^1$H decoupling ($\gamma B_1/2\pi = 100$ kHz) was used during acquisition, the transverse magnetization evolution, and refocusing periods. Relaxation and buildup time constants were then obtained by least-squares fitting of the data with a single-exponential function. The nuclear spin−lattice relaxation time constant ($T_{1I}$) and the DNP buildup constant ($T_B$) were measured by applying a presaturation pulse train consisting of 16 pulses with a flip angle of 108° and $\gamma B_1/2\pi = 50$ kHz (phase alternating along $+x$ and $+y$) separated by 5 ms on the $^1$H/$^{13}$C/$^{59}$Co channel. This was followed by a variable recovery time during which the longitudinal magnetization was allowed to build up. The polarization was then read out using a Bloch decay (for $^{13}$C and $^{59}$Co) or $^{13}$C{$^1$H} CP (for $^1$H). A time period of typically $1.3 \times T_{1I}$ ($T_B$) was allowed for polarization to build up prior to the read-out pulses (Table S2 in the Supporting Information). [98]

**Data Processing.** $^{59}$Co NMR parameters were simulated using the WSOLIDS software package.[99] Crystalline figures were made with Mercury[100] and the UCSF Chimera package.[101] EPR spectra were simulated using the Easyspin package.[102]

## RESULTS AND DISCUSSION

The pulsed 140 GHz EPR spectrum at 80 K (the same temperature as in the DNP experiments) of 0.1% Cr(III)-doped $[Co(en)_3Cl_3]_2{\cdot}NaCl{\cdot}6H_2O$ is shown in Figure 2. The shape of the spectrum can be explained using a spin Hamiltonian including the electron Zeeman interaction and the zero-field splitting of the $S = {}^3/_2$ system:

$$\hat{H}_{EPR} = \frac{g\mu_B B_0}{\hbar}\hat{S}_z + \hat{\mathbf{S}}\cdot\mathbf{D}\cdot\hat{\mathbf{S}} \quad (1)$$


dx.doi.org/10.1021/ja5044374 | J. Am. Chem. Soc. 2014, 136, 11716−11727

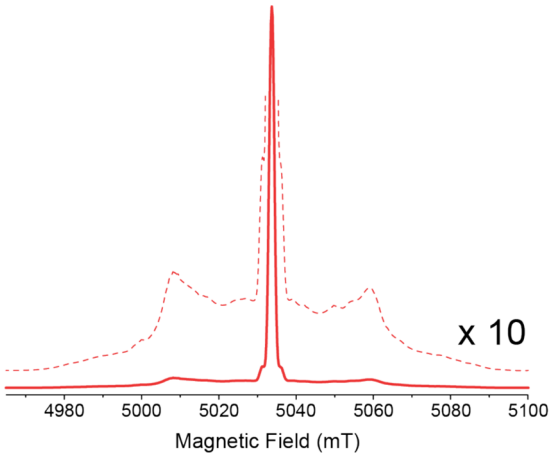


**Figure 2.** 140 GHz EPR spectrum of 0.1% Cr(III)-doped $[Co(en)_3Cl_3]_2{\cdot}NaCl{\cdot}6H_2O$. The spectrum was recorded by detecting the Hahn echo intensity as a function of the external magnetic field at a temperature of 80 K. The pulse sequence ($^{\pi}/_2$–$\tau$–$\pi$) was 13–200–26 ns, and 400 shots were recorded with a four-step phase cycle over 701 field points during a single field sweep. The dashed line shows a 10× vertical magnification to emphasize the anistropically broadened $m_S = \pm^3/_2 \leftrightarrow \pm^1/_2$ transitions.

where $g$ is the (isotropic) electronic $g$ factor; $\mu_B$ is the Bohr magneton; $\hbar$ is the reduced Planck constant; $\hat{\mathbf{S}}$ is the electron spin vector operator, constituted of the operator matrices according to $\hat{\mathbf{S}}^T = (\hat{S}_x, \hat{S}_y, \hat{S}_z)$; and $\mathbf{D}$ is the traceless ZFS tensor, typically expressed by its characteristic parameters $D = {}^3/_2 D_{zz}$ and $E = {}^1/_2(D_{yy} - D_{xx})$. The latter parameter can be omitted in eq 1 because the corresponding term is active only in tensor symmetries lower than axial. Since chromium in its natural isotopic composition features the magnetically active nucleus $^{53}$Cr with 9.5% abundance, a second spin system with the same terms as above but with an additional hyperfine coupling term $\hat{H}^{^{53}Cr}_{HFI} = a(^{53}Cr)\hat{\mathbf{S}}{\cdot}\hat{\mathbf{I}}$ has to be simulated and added to eq 1 with the appropriate weight. In the above term, $a(^{53}Cr)$ is the isotropic hyperfine coupling to $^{53}$Cr while $\hat{\mathbf{I}}$ is the nuclear spin vector operator, constituted of the operator matrices according to $\hat{\mathbf{I}}^T = (\hat{I}_x, \hat{I}_y, \hat{I}_z)$.

The spectrum is dominated by the $m_S = -^1/_2 \leftrightarrow +^1/_2$ CT of the $Cr^{3+}$ ion, but the anisotropically broadened $m_S = \pm^3/_2 \leftrightarrow \pm^1/_2$ transitions are visible as a Pake pattern centered around the CT. Spectral simulation using the EasySpin package[102] allowed us to determine $g = 1.98712$ and $D = +740$ MHz ($E = 0$ MHz); the sign of the ZFS constant $D$ is unambiguously defined on the basis of the slight asymmetry of the Pake pattern caused by the ∼15% Boltzmann population difference of the respective transitions and was confirmed by spectral simulation (Figure S1 in the Supporting Information). Although the occurrence of a significant ZFS may not be expected for the case of ideal hexagonal symmetry, distortion of the trigonal-antiprismatic ligand field is frequently observed in similar systems such as ruby; additionally, spin–orbit coupling generates an admixture of mainly the $^4T_2$ excited state to the $^4A_2$ electronic ground state, leading to the observed shift in $g$ with respect to that of a free electron and a nonvanishing ZFS.[103]

While the $g$ value is in relatively good agreement with the value of 1.9874 reported by McGarvey[86] (especially considering the low field of ∼340 mT where the previous experiments were performed), in our 80 K experiment $D$ is considerably larger than at room temperature (740 vs 148 MHz). Experiments performed at 9.7 GHz and 80 K confirmed our findings and also emphasized the significantly higher accuracy in the $g$ value determination provided by our high-field measurements (see Figure 3). The higher accuracy is attributed not only to the

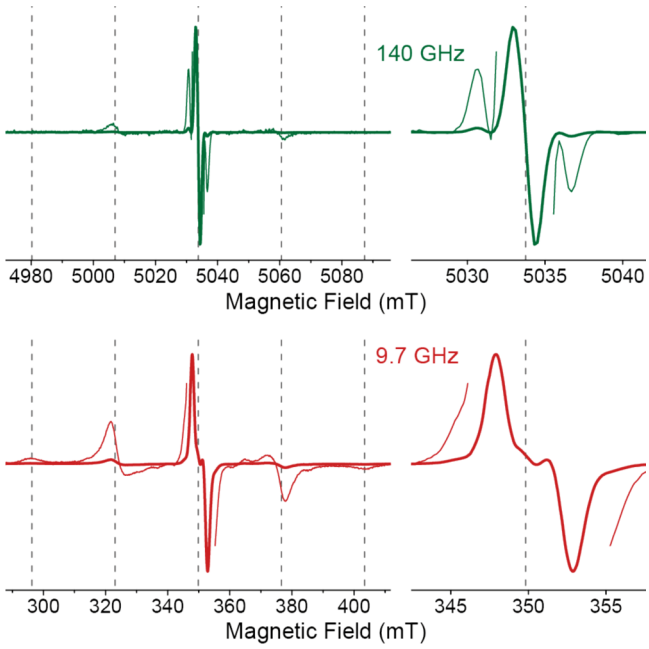


**Figure 3.** 140 GHz (top, green) and 9.7 GHz (bottom, red) EPR spectra of 0.1% Cr(III)-doped $[Co(en)_3Cl_3]_2{\cdot}NaCl{\cdot}6H_2O$ at a temperature of 80 K. The 140 GHz spectrum was obtained from the pulsed spectrum shown in Figure 2 by a mathematical pseudofield-modulation derivation (using EasySpin's fieldmod function[102]) with a pseudomodulation amplitude of 0.05 mT. The 9.7 GHz spectrum was recorded using CW EPR at a microwave power of 20 $\mu$W with field modulation of 0.2 mT in amplitude and 100 kHz in frequency; 2048 points were recorded with a time constant of 40.96 ms and a conversion time of 81.92 ms in a single sweep. The thin lines show 10× vertical magnifications to emphasize weak spectral features. The five equidistant dashed lines represent the positions of the prominent ZFS features and serve only as guides to the eyes.

larger Zeeman splitting but also to the reduction in the second-order ZFS broadening of the CT at higher magnetic fields. In the 140 GHz spectrum it is also easy to observe the outermost peaks of the hyperfine splitting quartet $[a(^{53}Cr) = 45$ MHz] of the ∼10% abundant $^{53}$Cr nucleus, while those peaks are completely masked by the second-order ZFS at 9.7 GHz (Figure 3).

In Figure 4 we illustrate that variation of the Cr(III) doping ratio has no impact on either the $g$ value or the $D$ value, indicating that both the crystal structure and properties are preserved and that the Cr(III) sites are not affected by an increase in the molar ratio of the paramagnetic dopant to 3%. Besides a gradual increase in mostly homogeneous line width due to stronger electron–electron interactions between different Cr(III) doping sites with increasing doping ratio, distinct shoulders emerge only in the EPR spectrum of the sample with a 3% doping ratio. These shoulders (marked with asterisks) show an offset of ∼250 MHz with respect to the CT, being in reasonable agreement with nearest-neighbor electron–electron coupling to a Cr(III) dopant at an adjacent complex site.


dx.doi.org/10.1021/ja5044374 | J. Am. Chem. Soc. 2014, 136, 11716–11727

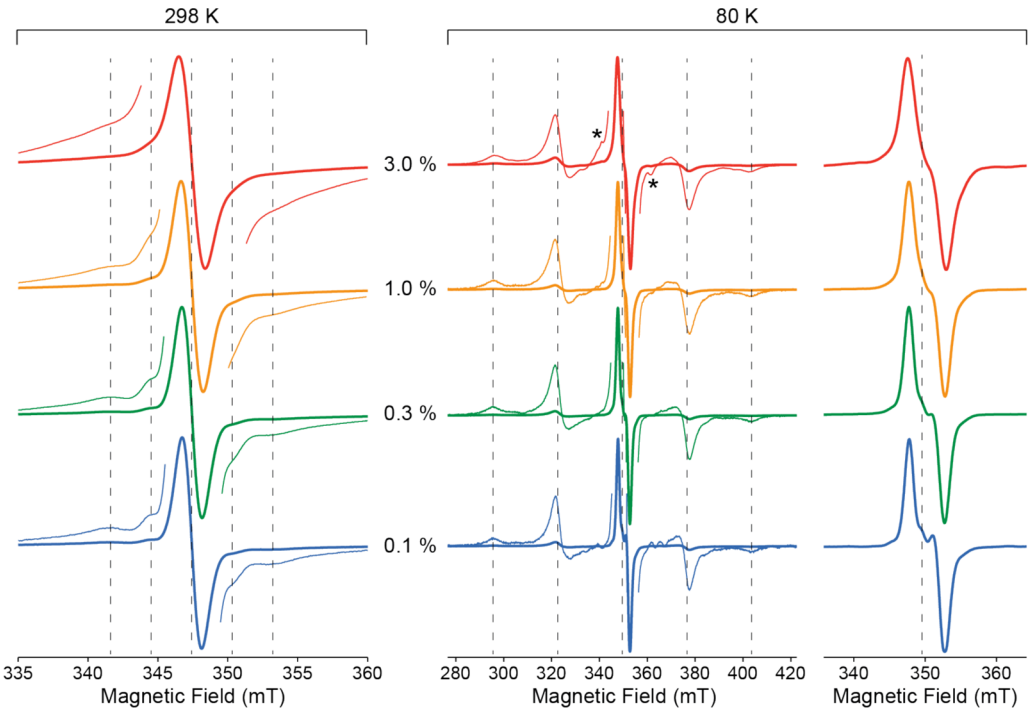


**Figure 4.** CW X-band EPR spectra of Cr(III)-doped $[Co(en)_3Cl_3]_2{\cdot}NaCl{\cdot}6H_2O$ with doping ratios of 0.1% (blue), 0.3% (green), 1.0% (orange), and 3.0% (red) recorded at sample temperatures of 298 K (left series) and 80 K (middle and right series). The series to the right depicts an enlarged region of the CT of the $S = {}^3/_2$ spin system at 80 K to visualize the features introduced by second-order ZFS. Thin lines show 7.5× amplifications to emphasize the weaker spectral features. The five equidistant dashed lines represent the positions of the prominent ZFS features and serve only as guides to the eyes. The 80 K (298 K) data were recorded using a microwave power of 0.2 $\mu$W (0.63 mW) and field modulation of 0.2 mT (0.1 mT) in amplitude and 100 kHz in frequency; 2048 (1024) points were recorded with a time constant of 40.96 (20.48) ms and a conversion time of 81.92 (40.96) ms in 1 to 24 scans depending on the doping ratio and temperature. Asterisks mark shoulders of the 3% Cr-doped complex that indicate nearest-neighbor electron−electron coupling.

Variable-temperature continuous-wave (CW) EPR spectra obtained from the 0.1% Cr(III)-doped sample (Figure 5) reveal a strong temperature dependence of the ZFS. Spectral simulation using the EasySpin package allowed us to extract the ZFS constant $D$ as a function of sample temperature (Figure 6). While $D$ reaches a plateau value of 840 MHz at temperatures below 20 K, its magnitude decreases almost linearly with increasing temperature above 40 K, reaching a value of ∼186 MHz at 320 K; the axial ZFS tensor symmetry is conserved throughout the whole accessible temperature range. While the occurrence of a nonvanishing ZFS in such a system is necessarily caused by the distortion from hexagonal symmetry,[104] its variation with temperature is less trivial to explain; however it can be generally attributed to coupling of the paramagnetic ion to temperature-induced lattice vibrations.[105,106] A significant temperature dependence in $D$ has been thoroughly documented with experiment and theory on systems such as MgO:$Cr^{3+}$ and ruby, and has been attributed to lattice expansion and electron−phonon interactions.[107−111] However, in these cases the absolute value of $D$ was much larger than in our system and increased only slightly in magnitude with increasing temperature (for $Cr^{3+}$ in ruby, the low-temperature value is $|D| \approx 5.7$ GHz, and the value increases by only ∼90 MHz over the range of 600 K).[108] Misra et al.[112] investigated the EPR properties of $[Cr(H_2O)_6]^{3+}$ in guanidinium aluminum sulfate hexahydrate and reported values of $D$ = −1164 and −892 MHz for the two different $Cr^{3+}$ lattice sites at 1.6 K, which decreased in absolute value to $D$ = −732 and −585 MHz, respectively, at 298 K. These values were later confirmed theoretically by Pan et al.[113] and explained in terms of a trigonal distortion of the hexagonal $Cr^{3+}$ site due to a slight mismatch of the ionic radii of $Al^{3+}$ (0.535 Å)[85] and $Cr^{3+}$ (0.615 Å), which causes an elongated distortion around the $Cr^{3+}$. In our case, the measured $D$ values are of opposite sign but very similar in absolute value, which decreases with increasing temperature. This suggests that a comparable situation arises here. Since the difference between the ionic radii of $Co^{3+}$ (0.545 Å) and $Cr^{3+}$ is slightly smaller than in the case of $Al^{3+}$, a smaller distortion and hence a smaller ZFS would arise. However, because of the difference in the crystal structures of the two host systems, the geometry of the distortion would be opposite (i.e., prolate vs oblate), as indicated by the opposite sign of the ZFS constant.

The $^1H$ enhancement factor $\varepsilon(^1H)$ (i.e., the ratio of the intensities of the DNP-enhanced and nonenhanced NMR spectra) shows only a minor variation as a function of the $Cr^{3+}$ doping ratio. All of the $^1H$ enhancement factors are on the order of 2−3, with a slight tendency for larger $\varepsilon(^1H)$ at the lowest chromium concentration (Figure 7). This is surprising because previous SE DNP experiments have shown a significant dependence of the enhancement factor on the concentration of the polarizing agent.[114] As a comparison, a simple calculation using the density $\rho$ = 1.567 g $cm^{-3}$ yields a $Cr^{3+}$ concentration of 36.2 mM for a doping ratio of 1 mol %. On the basis of this estimate and our experience with frozen solutions of polarizing agent radicals and transition-metal complexes, we expected to observe a maximum $\varepsilon(^1H)$ at a doping ratio of ∼0.3−1 mol % (i.e., a concentration of 10.9−36.2 mM). The polarization buildup and longitudinal relaxation time constants were strongly dependent on the doping ratio, ranging from ∼0.3 s


dx.doi.org/10.1021/ja5044374 | J. Am. Chem. Soc. 2014, 136, 11716−11727

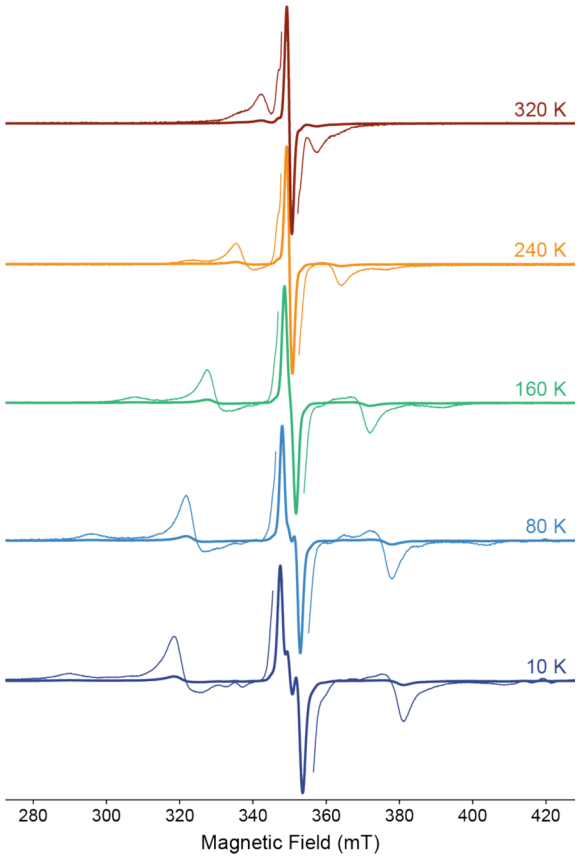


**Figure 5.** CW X-band EPR spectra of Cr(III)-doped $[Co(en)_3Cl_3]_2 \cdot NaCl \cdot 6H_2O$ with a doping ratio of 0.1% recorded at sample temperatures between 10 and 320 K. Thin lines show 10× vertical magnifications to emphasize the weaker spectral features. The data were recorded using a microwave power of 0.02−20 $\mu$W and field modulation of 0.2 mT in amplitude and 10−100 kHz in frequency; 2048 points were recorded with a time constant of 40.96 ms and a conversion time of 81.92 ms in a single sweep.

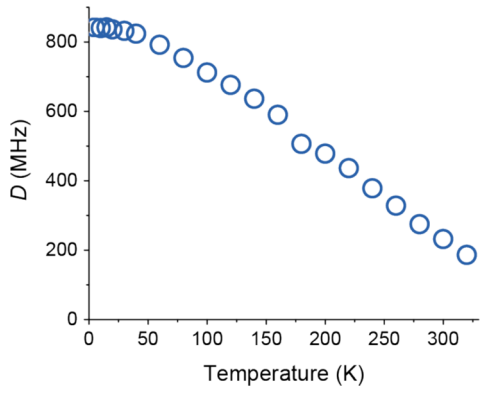


**Figure 6.** Zero-field splitting constant $D$ as a function of sample temperature. $D$ was obtained by spectral simulation of the EPR spectra (see representative selection in Figure 5) of 0.1% Cr(III)-doped $[Co(en)_3Cl_3]_2 \cdot NaCl \cdot 6H_2O$ using the EasySpin package.[102] Axial symmetry of the ZFS tensor was assumed for the simulations.

for 3 mol % up to 20 s for 0.1 mol %; in comparison, $T_{1I}$ for the undoped sample was measured to be as long as ∼200 s. The modest $\varepsilon(^1H)$ together with the unexpected polarizing agent concentration dependence indicates that the properties of the $^1H$ matrix in the crystal lead to very different behavior

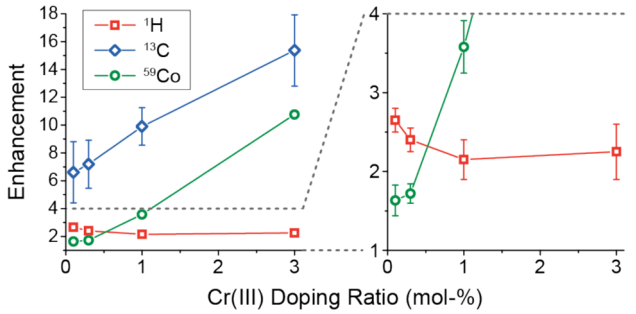


**Figure 7.** 211 MHz/140 GHz DNP enhancements obtained for $^1H$ (red squares), $^{13}C$ (blue diamonds), and $^{59}Co$ (green circles). Data were obtained as ratios of the NMR signal intensities with and without ∼5 W microwave irradiation at 80 K with MAS at 4 kHz. For the $^1H$ enhancements, the polarization was measured indirectly (i.e., $e^-$ to $^1H$ to $^{13}C$ via CP) at a magnetic field of 5027.6 mT, while for $^{13}C$ and $^{59}Co$ the direct polarization (i.e., $e^-$ to $^{13}C$ or $^{59}Co$) was measured during a Bloch decay ($^{13}C$) and a Hahn echo ($^{59}Co$) at a magnetic field of 5021.8 mT; the field values correspond to the expected SE DNP matching conditions. Polarization was read out after a buildup period of roughly $1.3T_B$. Error bars smaller than the data points have been omitted. The right graph shows an enlarged vertical scale.

compared with an amorphous, paramagnetically doped glass. Furthermore, the crystalline sample investigated in this study was constituted from natural-isotopic-abundance compounds, so it features a proton density of about 71 M, similar to the value of ∼100 M for 60/40 (v/v) glycerol/water. The proton concentration has already been shown to have a significant impact on DNP performance.[10,32] The effect of sample morphology on the DNP performance has also been discussed in the literature. In cases where the polarizing agent is dissolved, it has been shown that the formation of a glass upon freezing is crucial because the formation of solvent crystals would lead to phase segregation of the two immiscible solids (i.e., the solvent matrix and the polarizing agent).[24,28] In our case, however, the paramagnetic Cr(III) dopant is incorporated into the Co(III) host lattice during crystal growth, as confirmed by the EPR results (vide supra), and does not undergo phase separation with a change in temperature.

Both the $^{13}C$ and $^{59}Co$ DNP enhancements increased monotonically with increasing doping ratio. At 3% Cr(III), maximum enhancement factors of 16 (Figure S2 in the Supporting Information) and ∼11, respectively, were attained at a microwave power of 5 W (Figure 7) with buildup time constants on the order of ∼48 and 7 s, respectively. The $^{13}C$ DNP MAS NMR line width increased up to 15% with a Cr loading of 1% (vs 0% Cr at 83 K), which is reasonable for high-resolution work. Paramagnetic broadening became a significant issue when 3% Cr was used, whereby the line width increased by 40% (Table S3 in the Supporting Information). Therefore, further gains may be achieved at higher Cr loadings (vide supra), but care must be taken because the spectral resolution may be reduced by high paramagnetic metal cation concentration. In addition to paramagnetic relaxation, further complications may arise when large amounts of paramagnetic metals are used because hyperfine interactions (scaler and dipolar) may shift and split the resonances, as seen in other chemical systems.[56,115−121]

In principle, under the conditions faced in this study two different solid-state DNP mechanisms can be active with an inhomogeneously broadened EPR line: the solid effect (SE) and the cross effect (CE). The SE is active when the overall


dx.doi.org/10.1021/ja5044374 | J. Am. Chem. Soc. 2014, 136, 11716−11727

width of the EPR transition, constituted by the inhomogeneous breadth $\Delta$ and the homogeneous line width $\delta$, is smaller than the nuclear Larmor frequency: $\Delta, \delta < \omega_{0I}/2\pi$.[122−124] DNP enhancements of opposite sign are then observed at magnetic fields where the sum and the difference of the electron Larmor frequency $\omega_{0S}$ and the nuclear Larmor frequency $\omega_{0I}$ match the microwave frequency $\omega_{mw}$ (i.e., DNP enhancement can be achieved when the SE matching condition $\omega_{mw} = \omega_{0S} \pm \omega_{0I}$ is satisfied). On the other hand, the CE is active when $\delta < \omega_{0I}/2\pi < \Delta$, and cross-relaxation between two dipole−dipole-coupled electron spins can induce electron−electron−nuclear flip-flop-flips when $|\omega_{0S,1} - \omega_{0S,2}| = \omega_{0I}$.[125−129] Whereas in the case of $^{1}$H DNP it is quite clear that the SE should be the dominant DNP mechanism because $\omega_{0I}/2\pi = 214$ MHz > $\Delta = 40$ MHz and the accordingly chosen matching field, for $^{13}$C ($^{59}$Co) we face the situation where $\omega_{0I}/2\pi = 53$ (51) MHz $\approx \Delta = 40$ MHz. This does not allow us to determine straightforwardly which DNP mechanism will be active; on the contrary, SE and CE will be active at the same time with varying weights that depend on the polarizing agent concentration and microwave irradiation power. The situation of SE and CE occurring in parallel has been reported in the literature numerous times, especially for DNP of low-$\gamma$ nuclei.[25,31,36,130−132] In order to assess the contributions of the SE and the CE to the DNP, we recorded the field and power dependences of the DNP enhancements for the 3% Cr(III) sample. In Figure 8 the relevant part of the 140 GHz EPR spectrum is shown, together with vertical dashed lines indicating the positions of the center of the CT (red) and the $^{13}$C (blue) and $^{59}$Co (green) double- and zero-quantum resonance fields representing the SE matching fields. The field-dependent enhancement profiles clearly show positive and negative enhancement maxima that are closer to the CT than would be expected for the SE alone. At the same time, the power dependence of the $^{13}$C and $^{59}$Co enhancements (shown in the Figure 8 inset) indicates that the slope is smaller than in the nearly linear power dependence that has been observed for the SE in previous experiments.[32,34] The effect is more pronounced in the case of $^{13}$C; however, it is still significant for $^{59}$Co as well. These observations lead us to conclude that the CE plays an important role in reaching the experimental enhancement factors for the large doping ratio of 3%, which corresponds to a polarizing agent concentration of ∼110 mM. The strong dependence of $\varepsilon$ on the doping ratio supports this conclusion, as the CE becomes more and more efficient as the interelectronic distance is reduced and the dipole coupling between different Cr(III) centers is increased, therefore allowing more efficient electron−nuclear cross-relaxation (Table 1).

Even though the experimental observations clearly indicate a significant CE contribution, the exact mechanism that allows energy-conserving electron−electron−nuclear cross-relaxation is unclear. In amorphous solids, the required frequency difference between the electron spins is typically caused by a sufficiently large $g$ anisotropy and a random orientation of the radical molecules. In the present system, the $g$ factor is essentially isotropic, and the apparent line width of the CT should not allow for an efficient CE. Moreover, since in the crystalline system the molecular frames of all relevant interactions are identical for all centers within one crystallite,[86] orientational heterogeneity cannot lead to the necessary frequency matching, in contrast to amorphous systems. However, in a system of two $S = {}^{3}/_{2}$ spins and one $I = {}^{1}/_{2}$ nucleus, level degeneracies can be identified for certain

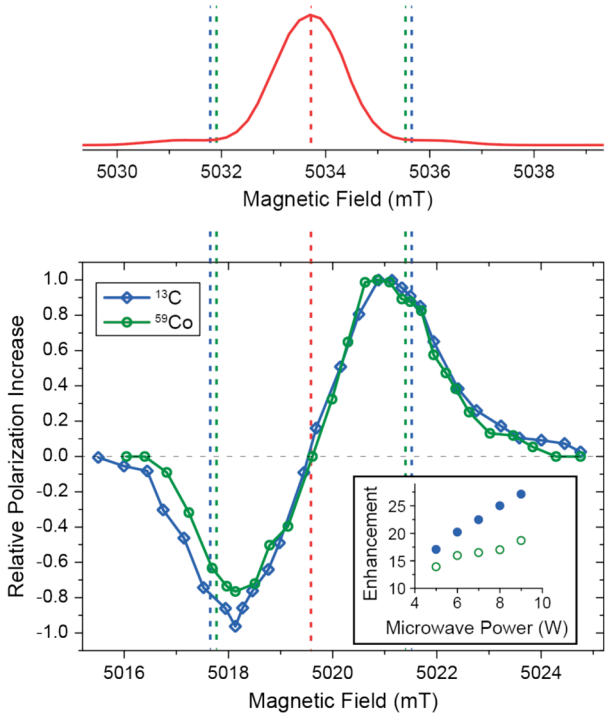


**Figure 8.** Normalized field-dependent DNP enhancements of $^{13}$C (blue diamonds) and $^{59}$Co (green circles) in 3% Cr(III)-doped $[Co(en)_3Cl_3]_2{\cdot}NaCl{\cdot}6H_2O$ measured under 8 W of 140 GHz microwaves with 4 kHz MAS at 80 K. The data were recorded by measuring the spin polarization after constant buildup periods of 50 and 10 s using Bloch decay and Hahn echo sequences for $^{13}$C and $^{59}$Co, respectively. The 140 GHz EPR spectrum (see Figure 2 for details) is shown at the top for comparison. The abscissa is on the same scale but has been shifted because of the slightly different frequencies of the microwave sources used for EPR and DNP. Dashed lines indicate the center of the EPR resonance (red) as well as the respective matching conditions for $^{13}$C (blue) and $^{59}$Co (green). The inset shows the microwave power dependence measured at the field of maximum enhancement.

**Table 1. Electron Distributions in $[Co(en)_3Cl_3]_2{\cdot}NaCl{\cdot}6H_2O$ Crystals with Increasing Paramagnetic Doping of $Cr^{3+}$**

| crystal | Cr (mol %) | $[Cr^{3+}]$ (mM) | $Cr^{3+}-Cr^{3+}$ distance (nm) |
|---|---|---|---|
| $[Co(en)_3Cl_3]_2{\cdot}NaCl{\cdot}6H_2O$ | 0 | 0.0 | n.a. |
| | 0.1 | 3.6 | 7.7 |
| | 0.3 | 10.9 | 5.3 |
| | 1 | 36.2 | 3.6 |
| | 3 | 108.6 | 2.5 |
| $[Cr(en)_3Cl_3]_2{\cdot}NaCl{\cdot}6H_2O$ | 100 | 3,650.0[a] | 0.8[a] |

[a]Based on Co derivative crystalline lattice parameters.

orientations of the ZFS tensor that allow for energy conserving flip-flop-flips for crystallites in specific orientations with respect to the external magnetic field. This can be demonstrated by analyzing a minimal spin Hamiltonian for such a system:

$$\hat{H}_{CE}^{ZFS} = \omega_{0S}(\hat{S}_{z,1} + \hat{S}_{z,2}) - \omega_{0I}\hat{I}_z + D\frac{3\cos^2\theta - 1}{2}\left[\hat{S}_{z,1}^2 + \hat{S}_{z,2}^2 - \frac{2}{3}S(S+1)\right] \quad (2)$$


dx.doi.org/10.1021/ja5044374 | J. Am. Chem. Soc. 2014, 136, 11716−11727

It should be noted that this Hamiltonian has been reduced to include only interactions leading to significant shifts in the eigenenergies of the system and does not represent all of the interactions required for the CE. Furthermore, it has been simplified with first-order perturbation theory; the introduction of higher-order terms does not lead to a qualitative change in the situation. The eigenenergies of this system can be calculated as

$$\frac{\varepsilon(m_{S,1}, m_{S,2}, m_I)}{\hbar} = (m_{S,1} + m_{S,2})\omega_{0S} - m_I\omega_{0I} + D\frac{(3\cos^2\theta - 1)}{2}\left[{m_{S,1}}^2 + {m_{S,2}}^2 - \frac{2}{3}S(S+1)\right] \quad (3)$$

Here it becomes obvious that two cases of degeneracies between states $|m_{S,1}, m_{S,2}, m_I\rangle$ in different $m_I$ subsets can be obtained: (1) for $D(3\cos^2\theta - 1) = \omega_{0I}$, the states $|-^3/_2, +^1/_2, +^1/_2\rangle$ and $|+^1/_2, -^3/_2, +^1/_2\rangle$ are strongly mixed with the state $|-^1/_2, -^1/_2, -^1/_2\rangle$, and mixing also occurs between $|+^1/_2, +^1/_2, -^1/_2\rangle$ and $|+^3/_2, -^1/_2, +^1/_2\rangle$ as well as $|-^1/_2, +^3/_2, +^1/_2\rangle$; (2) for $2D(3\cos^2\theta - 1) = \omega_{0I}$, the states $|\pm^1/_2, \mp^1/_2, -^1/_2\rangle$ are strongly mixed with $|\pm^3/_2, \mp^3/_2, +^1/_2\rangle$. The situation is similar when a nucleus with $I > {}^1/_2$ is considered, but larger shifts in nuclear Larmor frequency due to strong nuclear quadrupole interactions have to be included, while higher-order transitions with $\Delta m_I > 1$ may also play a role. As the ZFS is modulated by MAS, CE-enabling level crossings would occur for most crystallites during one rotor period as long as the orientation of the crystallite with respect to the spinning axis allows the matching conditions mentioned above to be achieved. Because of the smaller $\omega_{0I}$, this applies to more initial orientations for $^{13}$C and $^{59}$Co, while for $^1$H only a smaller ensemble of crystallites would be able to achieve matching. The theoretical importance of MAS-induced level crossings for the CE has recently been demonstrated;[133,134] crystalline systems like the one presently studied might be suitable systems for further systematic investigation of the practical implications.

Another matching condition can be described when one of the two electron spins is situated at a $^{53}$Cr nucleus. This situation is represented by the following spin Hamiltonian:

$$\hat{H}_{CE}^{ZFS} = \omega_{0S}(\hat{S}_{z,1} + \hat{S}_{z,2}) - \omega_{0I}\hat{I}_z + a(^{53}\mathrm{Cr})\hat{S}_{z,1}\hat{I}_z^{(^{53}\mathrm{Cr})} + D\frac{3\cos^2\theta - 1}{2}\left[\hat{S}_{z,1}^2 + \hat{S}_{z,2}^2 - \frac{2}{3}S(S+1)\right] \quad (4)$$

In eq 4, the additional terms with the index ($^{53}$Cr) are not to be confused with the nuclear spin parameters without the index: the latter represent the nucleus to be polarized, while the nuclear spin of $^{53}$Cr leads only to shifts in the eigenenergies of the first electron spin. The eigenenergies in this case are given by

$$\frac{\varepsilon(m_{S,1}, m_{S,2}, m_I)}{\hbar} = (m_{S,1} + m_{S,2})\omega_{0S} - m_I\omega_{0I} + a(^{53}\mathrm{Cr})m_{S,1}m_I^{(^{53}\mathrm{Cr})} + D\frac{3\cos^2\theta - 1}{2}\left[{m_{S,1}}^2 + {m_{S,2}}^2 - \frac{2}{3}S(S+1)\right] \quad (5)$$

This is analogous to the situation described above but allows for additional matching as a function of the $^{53}$Cr spin state. An interesting situation arises, however, when only the $m_{S,i} = \{-^1/_2, +^1/_2\}$ subspace is considered. In this subspace the ZFS can be neglected, since all of the levels experience the same ZFS shift. This leaves us with a reduced set of levels:

$$\frac{\varepsilon(m_{S,1}, m_{S,2}, m_I)}{\hbar} = (m_{S,1} + m_{S,2})\omega_{0S} - m_I\omega_{0I} + a(^{53}\mathrm{Cr})m_{S,1}m_I^{(^{53}\mathrm{Cr})} \quad \text{for } m_{S,i} = \left\{-\frac{1}{2}, +\frac{1}{2}\right\} \quad (6)$$

Here we can identify degeneracies under the condition $n|a(^{53}\mathrm{Cr})| = |\omega_{0I}|$ with $n = 1, 2, 3$ in the case of $I(^{53}\mathrm{Cr}) = {}^3/_2$. This is an interesting situation since it is not orientationally dependent and hence would always be active during MAS or nonspinning experiments. Also, since $\omega_{0I}(^{13}\mathrm{C}) \approx \omega_{0I}(^{59}\mathrm{Co}) \approx a(^{53}\mathrm{Cr})$ and $3a(^{53}\mathrm{Cr}) < \omega_{0I}(^1\mathrm{H})$, this effect could be active only for $^{13}$C and $^{59}$Co but not for $^1$H, which we observed. However, the limitations that both electrons have to be in the $m_{S,i} = \{-^1/_2, +^1/_2\}$ subspace and at least one electron must be situated at a $^{53}$Cr site leads to a reduced probability of finding matching pairs. Unfortunately, with the present data on hand, an unambiguous attribution of the dominant matching mechanism has not been successful.

Figure 9 shows a representative DNP-enhanced $^{59}$Co NMR signal for the compound containing 3% Cr(III) in comparison with a non-DNP-enhanced signal recorded under otherwise identical conditions. The enhancement factor in this case was ~11, which allowed us to acquire the above spectrum in 0.7 h ($T_B$ = 7.1 s, 256 scans, 45 $\mu$L sample volume). Longer DNP experiments (~4 h) revealed the separation of the $^{59}$Co satellite ($\pm^3/_2 \leftrightarrow \pm^1/_2$) peaks to be 4000−5000 ppm. In the non-DNP-enhanced spectra at 85 K these satellite transitions are difficult to observe, limiting the experimentalist's ability to determine the quadrupole coupling constant because of the noise even though the experiment was averaged for >14 h ($T_{1I}$ = 10 s, 4096 scans, 45 $\mu$L sample volume). By measurement of the separation between the satellites in the DNP-enhanced $^{59}$Co MAS NMR spectra (0.1 to 3% Cr), the quadrupole coupling constant and asymmetry parameter were determined to be $C_Q$ = 3.2 ± 0.3 MHz and $\eta$ < 0.1, respectively. At 85 K the molecular complex has an isotropic chemical shift ($\delta_{iso}$) of 7020 ppm, as determined by simulation of a series of nonspinning and MAS experiments (Figure S3 in the Supporting Information), a span ($\Omega$) of 525 ± 40 ppm, and a skew ($\kappa$) of >0.9. The change in temperature from 85 to 290 K has an effect on the $^{59}$Co chemical shielding parameters: in particular, $\delta_{iso}$ is shifted to a higher frequency of 7160 ppm (Figure 10) and $\Omega$ is reduced to 380 ± 25 ppm (Figure S3), as seen in similar $Co(en_3)Cl_3$ complexes (Table S4 in the

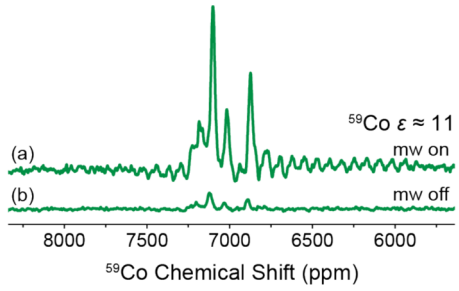


**Figure 9.** (a) DNP-enhanced and (b) non-DNP-enhanced $^{59}$Co NMR spectra of 3% Cr(III)-doped $[Co(en)_3Cl_3]_2{\cdot}NaCl{\cdot}6H_2O$ at 85 K recorded at 5021.8 mT (50.444 MHz) under 4 kHz MAS.


dx.doi.org/10.1021/ja5044374 | J. Am. Chem. Soc. 2014, 136, 11716−11727

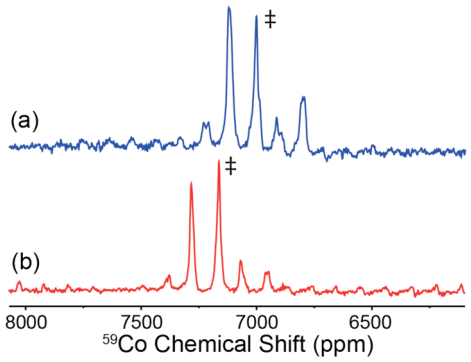


**Figure 10.** Comparison of $^{59}$Co MAS NMR spectra obtained at (a) 85 K (256 scans, DNP) and (b) 290 K (8192 scans, non-DNP) under MAS with a rotation frequency of 5.3 kHz. Spectra were acquired using an echo sequence at a field of 5.0218 T (50.44 MHz $^{59}$Co frequency) and are referenced to aqueous $K_3Co(CN)_6$.[88] The double dagger (‡) represents the $^{59}$Co isotropic chemical shift ($\delta_{iso}$).

Supporting Information) maintaining axial symmetry as required by crystal symmetry (vide supra).[65,88] The 140 ppm change in $\delta_{iso}$ and the increase in shielding span (at 85 K) are thought to be caused by changes within the lattice and the Co bonding character as one cools the DNP target; similar to the EPR effects described above. It should be noted that spectral changes have been reported previously when studying other challenging NMR nuclei using DNP, wherein both temperature and the solvent have affected the NMR parameters in nuclei that have considerable quadrupolar or chemical shielding interactions.[132,135]

## CONCLUSION

We have shown that significant DNP enhancements of $^{13}$C and $^{59}$Co can be achieved using Cr(III) as a paramagnetic dopant within a diamagnetic host lattice at a rather large molar doping ratio of 3%. Both the microwave power and field dependences suggest that the CE is at least partially involved as a DNP mechanism at this large paramagnet concentration. In contrast, polarization of $^1$H, where the SE is supposedly the active DNP mechanism, is limited to $\varepsilon \leq 3$. However, we emphasize that the experiments were performed on samples with natural-abundance isotopes, leaving a large potential for optimization of the proton concentration and Cr(III)/Co(III) doping ratio.

The $^{59}$Co NMR isotropic line width with DNP at cryogenic temperatures is not compromised compared with the NMR line width at room temperature using an undoped sample [i.e., 100% $Co(en_3)^{3+}$ complex] at 5 T. The maximum $^{59}$Co DNP enhancement factor ($\varepsilon$) of 19 at a microwave power of 9 W together with a ∼3.5-fold increase in Boltzmann polarization compared with room temperature leads to an overall signal enhancement of $\varepsilon^{\dagger}$ = 66. Doping of the crystalline lattice enables faster accumulation of transients as a result of shortening of $T_B$ and $T_{1I}$, which would otherwise be increased because of the use of cryogenic temperatures. High-field DNP NMR spectroscopy offers an ability to expand the area of challenging NMR nuclei that suffer from both quadrupolar and chemical shielding interactions, such as $^{59}$Co. The span of the $^{59}$Co CSA was increased by nearly 40% and shifted to lower frequency by 140 ppm relative to room temperature while maintaining axial symmetry, illustrating the sensitivity of $^{59}$Co to its local chemical environment.

The highly symmetrical system studied here clearly can be considered an idealized case to some degree. However, simple considerations show that the symmetry of the Cr(III) site can be significantly reduced without compromising the EPR line width and therefore the DNP efficiency. In our case, the symmetric environment imposes a ZFS constant of $D$ = 740 MHz under DNP conditions ($T$ = 80 K). At 140 GHz, this leads to an effective broadening of the CT by only about 10 MHz; the observed EPR line broadening of 40 MHz is likely dominated by unresolved hyperfine coupling to $^1$H. Therefore, we estimate that significant line broadening by second-order ZFS is of no practical concern unless $D$ reaches values on the order of 2 GHz (e.g., the maximum breadth of the second-order broadening effect on the CT for $D$ = 2.0 GHz and $S = {}^3/_2$ is ∼40 MHz at the commonly used DNP field of $B_0$ = 9.4 T). In a more general description, any paramagnetic metal with an effectively narrow EPR line may be used as a dopant in a similar manner as described in this study. Nevertheless, the applicability of dopants with larger line widths (exceeding the nuclear Larmor frequency) should not be ruled out per se, as the underlying effects are not yet fully understood and have to be individually investigated by experiment, especially for higher doping ratios, where the CE might become efficient.

## ASSOCIATED CONTENT

### Supporting Information

Spectral simulations, structural parameters, $T_{1I}$ and $T_B$ values, $^{13}$C CP MAS NMR isotropic line widths, and $^{59}$Co NMR parameters for $[Co(en)_3]Cl_3$-based complexes. This material is available free of charge via the Internet at http://pubs.acs.org.

## AUTHOR INFORMATION

### Corresponding Authors

rgg@mit.edu
claudioluchinat@cerm.unifi.it

### Present Addresses

[§]B.C.: Institute of Physical and Theoretical Chemistry, Institute of Biophysical Chemistry, and Center of Biomolecular Magnetic Resonance, Goethe University Frankfurt, Max-von-Laue-Str. 7, 60438 Frankfurt, Germany.
[‖]S.A.P. and A.A.S.: Department of Chemistry and Applied Biosciences, Laboratory of Physical Chemistry, ETH-Zürich, CH-8093 Zürich, Switzerland.

### Author Contributions

[⊥]B.C. and V.K.M. contributed equally.

### Notes

The authors declare no competing financial interest.

## ACKNOWLEDGMENTS

This paper is dedicated to the memory of Professor Ivano Bertini. The authors thank Loren B. Andreas, Ta-Chung Ong, Eugenio Daviso, C. Blake Wilson, Eric Keeler, Salima Bahri, Guido Pintacuda, and Prof. Fabrizio Mani for helpful discussions. We thank Jeffrey A. Bryant, Ronald DeRocher, Ajay Thakkar, and Mike Mullins for technical assistance. We greatly appreciate the help of Emilio A. Nanni, Sudheer K. Jawla, William C. Guss, Ivan Mastovsky, and Richard E. Temkin with the 140 GHz gyrotron and microwave components. We acknowledge financial support from the National Institutes of Health (EB002804 and EB002026). This work was supported by Ente Cassa di Risparmio di Firenze, MIUR-PRIN (2009FAKHZT and 2012SK7ASN), the European Commis-

sion (Contract Bio-NMR 261863), and the ESFRI Instruct Core Centre (CERM, Italy). B.C. was supported in part by the Deutsche Forschungsgemeinschaft (DFG Research Fellowship CO 802/1-1). V.K.M. is grateful to the Natural Sciences and Engineering Research Council of Canada and the Government of Canada for a Banting Postdoctoral Fellowship. E.R. acknowledges support from EMBO (ASTF-491/2013).

## REFERENCES

(1) Griffin, R. G.; Prisner, T. F. *Phys. Chem. Chem. Phys.* **2010**, *12*, 5737.
(2) Overhauser, A. W. *Phys. Rev.* **1953**, *92*, 411.
(3) Carver, T. R.; Slichter, C. P. *Phys. Rev.* **1953**, *92*, 212.
(4) Maly, T.; Debelouchina, G. T.; Bajaj, V. S.; Hu, K.-N.; Joo, C.-G.; Mak-Jurkauskas, M. L.; Sirigiri, J. R.; van der Wel, P. C. A.; Herzfeld, J.; Temkin, R. J.; Griffin, R. G. *J. Chem. Phys.* **2008**, *128*, No. 052211.
(5) Hu, K.-N.; Song, C.; Yu, H.-h.; Swager, T. M.; Griffin, R. G. *J. Chem. Phys.* **2008**, *128*, No. 052302.
(6) Hu, K.-N.; Debelouchina, G. T.; Smith, A. A.; Griffin, R. G. *J. Chem. Phys.* **2011**, *134*, No. 125105.
(7) Barnes, A. B.; De Paepe, G.; van der Wel, P. C. A.; Hu, K.-N.; Joo, C.-G.; Bajaj, V. S.; Mak-Jurkauskas, M. L.; Sirigiri, J. R.; Herzfeld, J.; Temkin, R. J.; Griffin, R. G. *Appl. Magn. Reson.* **2008**, *34*, 237.
(8) Akbey, Ü.; Franks, W. T.; Linden, A.; Lange, S.; Griffin, R. G.; van Rossum, B.-J.; Oschkinat, H. *Angew. Chem., Int. Ed.* **2010**, *49*, 7803.
(9) Lange, S.; Linden, A. H.; Akbey, Ü.; Franks, W. T.; Loening, N. M.; van Rossum, B.-J.; Oschkinat, H. *J. Magn. Reson.* **2012**, *216*, 209.
(10) Akbey, Ü.; Lange, S.; Franks, W. T.; Linser, R.; Rehbein, K.; Diehl, A.; van Rossum, B.-J.; Reif, B.; Oschkinat, H. *J. Biomol. NMR* **2010**, *46*, 67.
(11) Linden, A.; Franks, W. T.; Akbey, Ü.; Lange, S.; van Rossum, B.-J.; Oschkinat, H. *J. Biomol. NMR* **2011**, *51*, 283.
(12) Miéville, P.; Vitzthum, V.; Caporini, M. A.; Jannin, S.; Gerber-Lemaire, S.; Bodenhausen, G. *Magn. Reson. Chem.* **2011**, *49*, 689.
(13) van der Wel, P. C. A.; Hu, K.-N.; Lewandowski, J.; Griffin, R. G. *J. Am. Chem. Soc.* **2006**, *128*, 10840.
(14) Debelouchina, G. T.; Bayro, M. J.; van der Wel, P. C. A.; Caporini, M. A.; Barnes, A. B.; Rosay, M.; Maas, W. E.; Griffin, R. G. *Phys. Chem. Chem. Phys.* **2010**, *12*, 5911.
(15) Bayro, M. J.; Debelouchina, G. T.; Eddy, M. T.; Birkett, N. R.; MacPhee, C. E.; Rosay, M.; Maas, W. E.; Dobson, C. M.; Griffin, R. G. *J. Am. Chem. Soc.* **2011**, *133*, 13967.
(16) Gelis, I.; Vitzthum, V.; Dhimole, N.; Caporini, M.; Schedlbauer, A.; Carnevale, D.; Connell, S.; Fucini, P.; Bodenhausen, G. *J. Biomol. NMR* **2013**, *56*, 85.
(17) Rossini, A. J.; Zagdoun, A.; Hegner, F.; Schwarzwälder, M.; Gajan, D.; Copéret, C.; Lesage, A.; Emsley, L. *J. Am. Chem. Soc.* **2012**, *134*, 16899.
(18) Bajaj, V. S.; Mak-Jurkauskas, M. L.; Belenky, M.; Herzfeld, J.; Griffin, R. G. *Proc. Natl. Acad. Sci. U.S.A.* **2009**, *106*, 9244.
(19) Mak-Jurkauskas, M. L.; Bajaj, V. S.; Hornstein, M. K.; Belenky, M.; Griffin, R. G.; Herzfeld, J. *Proc. Natl. Acad. Sci. U.S.A.* **2008**, *105*, 883.
(20) Reggie, L.; Lopez, J. J.; Collinson, I.; Glaubitz, C.; Lorch, M. *J. Am. Chem. Soc.* **2011**, *133*, 19084.
(21) Lesage, A.; Lelli, M.; Gajan, D.; Caporini, M. A.; Vitzthum, V.; Miéville, P.; Alauzun, J.; Roussey, A.; Thieuleux, C.; Mehdi, A.; Bodenhausen, G.; Copéret, C.; Emsley, L. *J. Am. Chem. Soc.* **2010**, *132*, 15459.
(22) Andreas, L. B.; Barnes, A. B.; Corzilius, B.; Chou, J. J.; Miller, E. A.; Caporini, M.; Rosay, M.; Griffin, R. G. *Biochemistry* **2013**, *52*, 2774.
(23) Ravera, E.; Corzilius, B.; Michaelis, V. K.; Luchinat, C.; Griffin, R. G.; Bertini, I. *J. Phys. Chem. B* **2014**, *118*, 2957.
(24) Ravera, E.; Corzilius, B.; Michaelis, V. K.; Rosa, C.; Griffin, R. G.; Luchinat, C.; Bertini, I. *J. Am. Chem. Soc.* **2013**, *135*, 1641.
(25) Michaelis, V. K.; Ong, T.-C.; Kiesewetter, M. K.; Frantz, D. K.; Walish, J. J.; Ravera, E.; Luchinat, C.; Swager, T. M.; Griffin, R. G. *Isr. J. Chem.* **2014**, *54*, 207.
(26) Griffin, R. G. *Nature* **2010**, *468*, 381.
(27) Vitzthum, V.; Borcard, F.; Jannin, S.; Morin, M.; Miéville, P.; Caporini, M. A.; Sienkiewicz, A.; Gerber-Lemaire, S.; Bodenhausen, G. *ChemPhysChem* **2011**, *12*, 2929.
(28) Ong, T.-C.; Mak-Jurkauskas, M. L.; Walish, J. J.; Michaelis, V. K.; Corzilius, B.; Smith, A. A.; Clausen, A. M.; Cheetham, J. C.; Swager, T. M.; Griffin, R. G. *J. Phys. Chem. B* **2013**, *117*, 3040.
(29) Hovav, Y.; Feintuch, A.; Vega, S. *J. Chem. Phys.* **2011**, *134*, No. 074509.
(30) Smith, A. A.; Corzilius, B.; Barnes, A. B.; Maly, T.; Griffin, R. G. *J. Chem. Phys.* **2012**, *136*, No. 015101.
(31) Banerjee, D.; Shimon, D.; Feintuch, A.; Vega, S.; Goldfarb, D. *J. Magn. Reson.* **2013**, *230*, 212.
(32) Corzilius, B.; Smith, A. A.; Griffin, R. G. *J. Chem. Phys.* **2012**, *137*, No. 054201.
(33) Dane, E. L.; Corzilius, B.; Rizzato, E.; Stocker, P.; Maly, T.; Smith, A. A.; Griffin, R. G.; Ouari, O.; Tordo, P.; Swager, T. M. *J. Org. Chem.* **2012**, *77*, 1789.
(34) Haze, O.; Corzilius, B.; Smith, A. A.; Griffin, R. G.; Swager, T. M. *J. Am. Chem. Soc.* **2012**, *134*, 14287.
(35) Kiesewetter, M. K.; Corzilius, B.; Smith, A. A.; Griffin, R. G.; Swager, T. M. *J. Am. Chem. Soc.* **2012**, *134*, 4537.
(36) Michaelis, V. K.; Smith, A. A.; Corzilius, B.; Haze, O.; Swager, T. M.; Griffin, R. G. *J. Am. Chem. Soc.* **2013**, *135*, 2935.
(37) Hu, K.-N. *Solid State Nucl. Magn. Reson.* **2011**, *40*, 31.
(38) Matsuki, Y.; Maly, T.; Ouari, O.; Karoui, H.; Le Moigne, F.; Rizzato, E.; Lyubenova, S.; Herzfeld, J.; Prisner, T.; Tordo, P.; Griffin, R. G. *Angew. Chem., Int. Ed.* **2009**, *48*, 4996.
(39) Ysacco, C.; Karoui, H.; Casano, G.; Le Moigne, F.; Combes, S.; Rockenbauer, A.; Rosay, M.; Maas, W.; Ouari, O.; Tordo, P. *Appl. Magn. Reson.* **2012**, *43*, 251.
(40) Ysacco, C.; Rizzato, E.; Virolleaud, M.-A.; Karoui, H.; Rockenbauer, A.; Le Moigne, F.; Siri, D.; Ouari, O.; Griffin, R. G.; Tordo, P. *Phys. Chem. Chem. Phys.* **2010**, *12*, 5841.
(41) Zagdoun, A.; Casano, G.; Ouari, O.; Lapadula, G.; Rossini, A. J.; Lelli, M.; Baffert, M.; Gajan, D.; Veyre, L.; Maas, W. E.; Rosay, M.; Weber, R. T.; Thieuleux, C.; Coperet, C.; Lesage, A.; Tordo, P.; Emsley, L. *J. Am. Chem. Soc.* **2012**, *134*, 2284.
(42) Corzilius, B.; Smith, A. A.; Barnes, A. B.; Luchinat, C.; Bertini, I.; Griffin, R. G. *J. Am. Chem. Soc.* **2011**, *133*, 5648.
(43) Luchinat, C.; Parigi, G.; Ravera, E. *J. Biomol. NMR* **2013**, *57*, 155−166.
(44) Bencini, A.; Gatteschi, D. In *Transition Metal Chemistry*; Melson, G. A., Figgis, B. N., Eds.; Marcel Dekker: New York, 1983; Vol. *8*, p 1.
(45) Doyle, W. T. *Phys. Rev.* **1962**, *126*, 1421.
(46) Seidel, H. *Z. Physik* **1961**, *165*, 218.
(47) Holton, W. C.; Blum, H. *Phys. Rev.* **1962**, *125*, 89.
(48) Loubser, J. H. N.; van Wyk, J. A. *Rep. Prog. Phys.* **1978**, *41*, 1201.
(49) Waldherr, G.; Beck, J.; Steiner, M.; Neumann, P.; Gali, A.; Frauenheim, T.; Jelezko, F.; Wrachtrup, J. *Phys. Rev. Lett.* **2011**, *106*, No. 157601.
(50) Neumann, P.; Jakobi, I.; Dolde, F.; Burk, C.; Reuter, R.; Waldherr, G.; Honert, J.; Wolf, T.; Brunner, A.; Shim, J. H.; Suter, D.; Sumiva, H.; Isoya, J.; Wrachtrup, J. *Nano Lett.* **2013**, *13*, 2738.
(51) Brough, A. R.; Grey, C. P.; Dobson, C. M. *J. Am. Chem. Soc.* **1993**, *115*, 7318.
(52) Wickramasinghe, N. P.; Shaibat, M. A.; Ishii, Y. *J. Phys. Chem. B* **2007**, *111*, 9693.
(53) Huang, W.; Schopfer, M.; Zhang, C.; Howell, R. C.; Todaro, L.; Gee, B. A.; Francesconi, L. C.; Polenova, T. *J. Am. Chem. Soc.* **2008**, *130*, 481.
(54) Kervern, G.; D'Aléo, A.; Toupet, L.; Maury, O.; Emsley, L.; Pintacuda, G. *Angew. Chem., Int. Ed.* **2009**, *48*, 3082.
(55) Clément, R. J.; Pell, A. J.; Middlemiss, D. S.; Strobridge, F. C.; Miller, J. K.; Whittingham, M. S.; Emsley, L.; Grey, C. P.; Pintacuda, G. *J. Am. Chem. Soc.* **2012**, *134*, 17178.

(56) Michaelis, V. K.; Greer, B. J.; Aharen, T.; Greedan, J. E.; Kroeker, S. *J. Phys. Chem. C* **2012**, *116*, 23646.
(57) Bhaumik, A.; Luchinat, C.; Parigi, G.; Ravera, E.; Rinaldelli, M. *CrystEngComm* **2013**, *15*, 8639.
(58) Pregosin, P. S. *Transition Metal Nuclear Magnetic Resonance*; Elsevier: Amsterdam, 1991.
(59) MacKenzie, K. J. D.; Smith, E. *Multinuclear Solid-State Nuclear Magnetic Resonance of Inorganic Materials*; Elsevier Science: Oxford, U.K., 2002.
(60) Ardenkjær-Larsen, J. H.; Laursen, I.; Leunbach, I.; Ehnholm, G.; Wistrand, L. G.; Petersson, J. S.; Golman, K. *J. Magn. Reson.* **1998**, *133*, 1.
(61) Koelsch, C. F. *J. Am. Chem. Soc.* **1957**, *79*, 4439.
(62) Song, C.; Hu, K.-N.; Joo, C.-G.; Swager, T. M.; Griffin, R. G. *J. Am. Chem. Soc.* **2006**, *128*, 11385.
(63) Sauvée, C.; Rosay, M.; Casano, G.; Aussenac, F.; Weber, R. T.; Ouari, O.; Tordo, P. *Angew. Chem., Int. Ed.* **2013**, *52*, 10858.
(64) Mason, J. *Multinuclear NMR*; Plenum Press: New York, 1987; p 639.
(65) Kirby, C. W.; Power, W. P. *Can. J. Chem.* **2001**, *79*, 296.
(66) Crewdson, P.; Bryce, D. L.; Rominger, F.; Hofmann, P. *Angew. Chem., Int. Ed.* **2008**, *47*, 3454.
(67) Bryce, D. L.; Wasylishen, R. E. *Phys. Chem. Chem. Phys.* **2001**, *3*, 5154.
(68) Lo, A. Y. H.; Bitterwolf, T. E.; Macdonald, C. L. B.; Schurko, R. W. *J. Phys. Chem. A* **2005**, *109*, 7073.
(69) Kroeker, S.; Wasylishen, R. E. *Can. J. Chem.* **1999**, *77*, 1962.
(70) Forgeron, M. A. M.; Wasylishen, R. E. *Phys. Chem. Chem. Phys.* **2008**, *10*, 574.
(71) Sutrisno, A.; Terskikh, V. V.; Huang, Y. *Chem. Commun.* **2009**, 186.
(72) Michaelis, V. K.; Kroeker, S. *J. Phys. Chem. C* **2010**, *114*, 21736.
(73) Chen, F.; Ma, G.; Bernard, G. M.; Cavell, R. G.; McDonald, R.; Ferguson, M. J.; Wasylishen, R. E. *J. Am. Chem. Soc.* **2010**, *132*, 5479.
(74) Widdifield, C. M.; Bain, A. D.; Bryce, D. L. *Phys. Chem. Chem. Phys.* **2011**, *13*, 12413.
(75) Schurko, R. W. *Acc. Chem. Res.* **2013**, *46*, 1985.
(76) Bertini, I.; Luchinat, C.; Parigi, G. *Solution NMR of Paramagnetic Molecules: Applications to Metallobiomolecules and Models*; Elsevier: Amsterdam, 2001.
(77) Glättli, H.; Odehnal, M.; Ezratty, J.; Malinovski, A.; Abragam, A. *Phys. Lett. A* **1969**, *29*, 250.
(78) Stepanov, A. P.; Fedotov, V. N.; Baldin, V. I.; Yunosov, N. B. *Dokl. Akad. Nauk SSSR* **1970**, *194*, 871.
(79) Borghini, M.; Niinikoski, T. O.; Udo, F.; Weymuth, P. *Nucl. Instrum. Methods* **1972**, *105*, 215.
(80) De Boer, W. *Nucl. Instrum. Methods* **1973**, *107*, 99.
(81) Svoboda, J. *J. Phys. C* **1974**, *7*, L144.
(82) Svoboda, J. *Czech. J. Phys.* **1975**, *25*, 340.
(83) Guckelsberger, K. *Nucl. Instrum. Methods* **1977**, *144*, 93.
(84) Farrugia, L. J.; Peacock, R. D.; Stewart, B. *Acta Crystallogr, Sect. C* **2000**, *56*, 149.
(85) Shannon, R. D. *Acta Crystallogr, Sect. A* **1976**, *32*, 751.
(86) McGarvey, B. R. *J. Chem. Phys.* **1964**, *41*, 3743.
(87) Stone, N. J. *At. Data Nucl. Data Tables* **2005**, *90*, 75.
(88) Ueda, T.; Bernard, G. M.; McDonald, R.; Wasylishen, R. E. *Solid State Nucl. Magn. Reson.* **2003**, *24*, 163.
(89) Chan, J. C. C.; Au-Yeung, S. C. F. *Annu. Rep. NMR Spectrosc.* **2000**, *41*, 1.
(90) Nielsen, U. G.; Jakobsen, H. J.; Skibsted, J. *Solid State Nucl. Magn. Reson.* **2001**, *20*, 23.
(91) Ooms, K. J.; Bernard, G. M.; Kadziola, A.; Kofod, P.; Wasylishen, R. E. *Phys. Chem. Chem. Phys.* **2009**, *11*, 2690.
(92) Smith, A. A.; Corzilius, B.; Bryant, J. A.; DeRocher, R.; Woskov, P. P.; Temkin, R. J.; Griffin, R. G. *J. Magn. Reson.* **2012**, *223*, 170.
(93) Barnes, A. B.; Mak-Jurkauskas, M. L.; Matsuki, Y.; Bajaj, V. S.; van der Wel, P. C. A.; DeRocher, R.; Bryant, J.; Sirigiri, J. R.; Temkin, R. J.; Lugtenburg, J.; Herzfeld, J.; Griffin, R. G. *J. Magn. Reson.* **2009**, *198*, 261.
(94) Becerra, L. R.; Gerfen, G. J.; Temkin, R. J.; Singel, D. J.; Griffin, R. G. *Phys. Rev. Lett.* **1993**, *71*, 3561.
(95) Maly, T.; Bryant, J.; Ruben, D.; Griffin, R. G. *J. Magn. Reson.* **2006**, *183*, 303.
(96) Pines, A.; Gibby, M. G.; Waugh, J. S. *J. Chem. Phys.* **1972**, *56*, 1776.
(97) Bennett, A. E.; Rienstra, C. M.; Auger, M.; Lakshmi, K. V.; Griffin, R. G. *J. Chem. Phys.* **1995**, *103*, 6951.
(98) Pons, M.; Feliz, M.; Giralt, E. *J. Magn. Reson.* **1988**, *78*, 314.
(99) Eichele, K. *WSolids1 Software*, version 1.20.21; Universität Tübingen: Tübingen, Germany, 2013.
(100) Macrae, C. F.; Bruno, I. J.; Chisholm, J. A.; Edgington, P. R.; McCabe, P.; Pidcock, E.; Rodriguez-Monge, L.; Taylor, R.; van de Streek, J.; Wood, P. A. *J. Appl. Crystallogr.* **2008**, *41*, 466.
(101) Pettersen, E. F.; Goddard, T. D.; Huang, C. C.; Couch, G. S.; Greenblatt, D. M.; Meng, E. C.; Ferrin, T. E. *J. Comput. Chem.* **2004**, *25*, 1605.
(102) Stoll, S.; Schweiger, A. *J. Magn. Reson.* **2006**, *178*, 42.
(103) Kamimura, H. *Phys. Rev.* **1962**, *128*, 1077.
(104) Stout, E. W.; Garrett, B. B. *Inorg. Chem.* **1973**, *12*, 2565.
(105) Garrett, B. B.; Holbrook, M. T.; Stanko, J. A. *Inorg. Chem.* **1977**, *16*, 1159.
(106) Owens, F. J. *Phys. Status Solidi B* **1977**, *79*, 623.
(107) Zheng, W.-C.; Jia, G.-M.; He, L.; Yang, W.-Q. *Spectrochim. Acta, Part A* **2011**, *78*, 818.
(108) Klein, H.; Scherz, U.; Schulz, M.; Setyono, H.; Wisznewski, K. *Z. Phys. B* **1977**, *28*, 149.
(109) Ma, D.-P.; Chen, J.-R. *Commun. Theor. Phys.* **2005**, *43*, 529.
(110) Shrivastava, K. N. *Proc. R. Soc. London, Ser. A* **1988**, *419*, 287.
(111) Zheng, W.-C.; Wu, S.-Y. *Phys. Rev. B* **1996**, *54*, 1117.
(112) Misra, S. K.; Giguere, P.; Sharp, G. R. *J. Chem. Phys.* **1977**, *66*, 1758.
(113) Pan, L.-L.; Kuang, X.-Y.; Mao, A.-J.; Wang, H.; Huang, J.-L. *Chem. Phys. Lett.* **2007**, *442*, 468.
(114) Corzilius, B.; Andreas, L. B.; Smith, A. A.; Ni, Q. Z.; Griffin, R. G. *J. Magn. Reson.* **2014**, *240*, 113.
(115) Carlier, D.; Ménétrier, M.; Grey, C. P.; Delmas, C.; Ceder, G. *Phys. Rev. B* **2003**, *67*, No. 174103.
(116) Grey, C. P.; Smith, M. E.; Cheetham, A. K.; Dobson, C. M.; Dupree, R. *J. Am. Chem. Soc.* **1990**, *112*, 4670.
(117) Zhang, Y.; Gossman, W.; Oldfield, E. *J. Am. Chem. Soc.* **2003**, *125*, 16387.
(118) La Mar, G. N.; Horrocks, W. E.; Holm, R. H. *NMR of Paramagnetic Molecules*; Academic Press: New York, 1973.
(119) Aguiar, P. M.; Katz, M. J.; Leznoff, D. B.; Kroeker, S. *Phys. Chem. Chem. Phys.* **2009**, *11*, 6925.
(120) Cahill, L. S.; Yin, S. C.; Samoson, A.; Heinmaa, I.; Nazar, L. F.; Goward, G. R. *Chem. Mater.* **2005**, *17*, 6560.
(121) Ishii, Y.; Wickramasinghe, N. P.; Chimon, S. *J. Am. Chem. Soc.* **2003**, *125*, 3438.
(122) Abragam, A.; Proctor, W. G. *C. R. Acad. Sci.* **1958**, *246*, 2253.
(123) Abraham, M.; Jeffries, C. D.; Kedzie, R. W. *Phys. Rev.* **1960**, *117*, 1070.
(124) Abraham, M.; Kedzie, R. W.; Jeffries, C. D. *Phys. Rev.* **1957**, *106*, 165.
(125) Kessenikh, A. V.; Lushchikov, V. I.; Manenkov, A. A.; Taran, Y. V. *Soviet Phys.—Solid State* **1963**, *5*, 321.
(126) Hwang, C. F.; Hill, D. A. *Phys. Rev. Lett.* **1967**, *18*, 110.
(127) Hwang, C. F.; Hill, D. A. *Phys. Rev. Lett.* **1967**, *19*, 1011.
(128) Wollan, D. S. *Phys. Rev. B* **1976**, *13*, 3671.
(129) Wollan, D. S. *Phys. Rev. B* **1976**, *13*, 3686.
(130) Borghini, M.; de Boer, W.; Morimoto, K. *Phys. Lett. A* **1974**, *48*, 244.
(131) Shimon, D.; Hovav, Y.; Feintuch, A.; Goldfarb, D.; Vega, S. *Phys. Chem. Chem. Phys.* **2012**, *14*, 5729.
(132) Michaelis, V. K.; Corzilius, B.; Smith, A. A.; Griffin, R. G. *J. Phys. Chem. B* **2013**, *117*, 14894.
(133) Thurber, K. R.; Tycko, R. *J. Chem. Phys.* **2012**, *137*, No. 084508.

(134) Mentink-Vigier, F.; Akbey, Ü.; Hovav, Y.; Vega, S.; Oschkinat, H.; Feintuch, A. *J. Magn. Reson.* **2012**, *224*, 13.
(135) Gunther, W. R.; Michaelis, V. K.; Caporini, M. A.; Griffin, R. G.; Roman-Leshkov, Y. *J. Am. Chem. Soc.* **2014**, *136*, 6219.